Applied Catalysis B: Environmental 142–143 (2013) 196–204

Contents lists available at SciVerse ScienceDirect

Applied Catalysis B: Environmental

journal homepage: www.elsevier.com/locate/apcatb

Investigation of NO and NO_2 adsorption mechanisms on TiO_2 at room temperature

L. Sivachandiran[a,b,c], F. Thevenet[a,b,*], P. Gravejat[a,b], A. Rousseau[c]

[a] Université Lille Nord de France, F-59000 Lille, France
[b] Département Chimie et Environnement, Ecole des Mines de Douai, F-59508 Douai, France
[c] Laboratoire de Physique des Plasmas, Ecole Polytechnique, UPMC, Université Paris Sud 11, CNRS Palaiseau, France

ARTICLE INFO

Article history:
Received 21 February 2013
Received in revised form 26 April 2013
Accepted 30 April 2013
Available online 18 May 2013

Keywords:
Adsorption
TiO_2
NO_2
NO
NO_3

ABSTRACT

In this study, NO and NO_2 adsorption mechanisms on TiO_2 at room temperature have been investigated separately. Atmospheric pressure gas phase Fourier Transform Infrared Spectroscopy (FTIR) coupled to adsorption and temperature programmed desorption (TPD) experiments have been used to characterize gas phase and adsorbed phase species. TiO_2 coated glass beads packed-bed reactor has been designed and used for NO and NO_2 adsorption and storage capacity under dark and gas-flowing conditions at room temperature. For NO adsorption, experimental data suggests that, at room temperature, NO shows no significant adsorption on TiO_2. On the other hand NO_2 adsorbs in a reactive way by evolving NO in the gas phase. We quantitatively evidenced that, the ratio between consumed NO_2, desorbed NO_2 by TPD after adsorption and produced NO during NO_2 adsorption is 3:2:1, by a qualitative and quantitative analysis performed downstream the reactor. Based on the quantitative analysis, a new NO_2 adsorption mechanism on TiO_2 at room temperature has been proposed, and validated for various NO_2 inlet concentrations. The proposed mechanism is valid on the investigated NO_2 inlet concentration range. In addition, it was found that, NO formation time, during NO_2 adsorption, is rather controlled by TiO_2 surface coverage than NO_2 inlet concentration; similarly, adsorption time i.e. surface coverage, significantly modifies the nature of adsorbed species on TiO_2 surface.

1. Introduction

Since last two decades indoor air cleaning has attracted much attention owing to stringent air pollution control, consequently various pollution reduction processes were developed [1,2]. Among them adsorption, photocatalysis and Non Thermal Plasma technology (NTP) are the most studied methods [3–6]. The authors have reported the highest performance by coupling catalytic materials with NTP techniques [7]. Adsorption and desorption of pollutants from catalyst surface are key parameters in these heterogeneous techniques. For instance, adsorption makes possible the catalytic treatment of pollutants; moreover, it expands the residence time of compounds to be treated in plasma–catalyst combination. In addition, desorption of obtained products makes possible the renewal of pollutants on the surface. Nevertheless, in both photocatalytic and NTP-catalytic methods, the catalyst deactivation has been reported by several authors [8–10]. This phenomenon has been generally attributed to the irreversible adsorption of CO_X, NO_X and/or reactive intermediates on the catalyst surface [10,11]. Hence, desorption of strongly bonded species appears as a key point in the system sustainability.

Titanium dioxide (TiO_2) is a metal oxide widely associated with NTP, not only for its high relative permittivity, but, above all, for its catalytic and photocatalytic properties. Coupling of NTP with TiO_2 for Volatile Organic Compound (VOC) abatement or even chemical synthesis is mainly justified by TiO_2 surface properties of adsorption or complexation [6,12–14]. The understanding of physical chemistry involved in plasma–catalyst heterogeneous air treatment systems; requires knowledge improvements in pollutant adsorption phenomenon on commonly used materials. Thus, system performance and aging could be better understood.

NOx (NO and NO_2) are formed when nitrogen from air and fuels combine with oxygen at high temperatures for instance in thermal power plants, welding, and combustion engines. For diesel engines equipped with OEM (Original Equipment Manufacturer) particle filters, operating under urban driving conditions NO_2 accounts for 35–70% of total NOx gas emissions [15]. Besides, it is well reported that, when NTP is ignited in air (mixture of N_2/O_2) it produces higher oxides of Nitrogen compounds such as NO, N_2O, NO_2 and HNO_3 in concentration of several ppm to some hundred ppm depending on deposited energy [7,16,17]. Furthermore in NTP

* Corresponding author at: Département Chimie et Environnement, Ecole des Mines de Douai, F-59508 Douai, France. Tel.: +33 3 27 71 26 12; fax: +33 3 27 71 29 14.
E-mail address: frederic.thevenet@mines-douai.fr (F. Thevenet).

0926-3373/$ – see front matter © 2013 Elsevier B.V. All rights reserved.
http://dx.doi.org/10.1016/j.apcatb.2013.04.073

process under air, the major part of NOx contributes by NO_2 due to the rapid oxidation of NO with highly active Ozone produced by NTP [18].

The level of NO and NO_2 in indoor air are respectively in the range of several hundred ppb and less than a hundred ppb [19]. National Institute for Occupational Safety and Health (NIOSH) suggested that the Immediately Dangerous to Life and Health (IDLH) concentration of NO_2 is 20 ppm. Studies focused on risk assessment have shown that high outdoor NO_2 concentration observed in residential areas contributes to increased respiratory and cardiovascular diseases and mortality [20].

Therefore, in the case of air treatment systems by adsorption-photocatalysis or plasma–catalyst, VOCs are targeted compounds, but the metal oxide surface is exposed to the wide diversity of species present in the air stream or generated by the system itself. Among them, NOx may dramatically influence VOC adsorption processes and decomposition mechanisms [21,22], which may also impact the system efficiency and aging.

NO_2 is a radical molecule, with a high electron affinity [23] (2.3 eV). Therefore, on TiO_2 surface, it can react to the metal center namely Ti^{4+} sites through O, N, or a combination of both. Metal oxides are very efficient as sorbents or catalysts for trapping and/or converting NO_2 and other NO_X species [24–27]. Dalton et al. [28] have reported that, TiO_2 effectively converts NO_2 to harmless nitrates species under UV radiation in continuous flow reactor. In addition to that, authors have also confirmed the adsorbed NO peak along with nitrate species by XPS analysis on TiO_2 surface under 8.10^{-9} Torr total pressure. On the other hand, Dan et al. [29] have found that, NO adsorbs weakly on TiO_2 and desorbs around 127 K. However, metal oxides are used in NO_X storage technologies, where the release of NO_X at higher temperatures is a key issue [30]. Interestingly, there was no enough study on NO_X storage and quantification on TiO_2 with flowing condition, and under typical ambient indoor air conditions.

The objective of this study is to investigate the NO and NO_2 adsorption mechanisms and storage capacity on TiO_2 at room temperature and under dry air flowing conditions. Specific focus is given to propose a NO_2 reactive adsorption mechanism on TiO_2 at room temperature. In addition, the proposed mechanism is validated for various NO_2 gas phase concentrations.

2. Experimental description

The laboratory scale experimental system used to investigate the NOx adsorption mechanism on TiO_2 is schematically shown in Fig. 1. NO and NO_2 adsorption has been studied in a TiO_2 coated glass beads packed bed Pyrex-glass tube reactor.

As shown in Fig. 1, the experimental setup can be divided into three main parts: (i) gas stream preparation; (ii) adsorption reactor; and (iii) analytical device.

2.1. Gas stream preparation

NO and NO_2 are provided by Praxair (99.9% purity), concentrations are respectively 20 and 50 ppm and balanced in Nitrogen. Zero air, characterized by very low levels of CO, CO_2, VOC and moisture was produced by PSA (Pressure Swing adsorption) gas purifier (Parker, BALSTON) coupled with Claind AZ 2020 catalytic zero air generators. Remaining carbaneous impurities in the air flow are lower than the analytical system detection limits: VOC <100 ppt; CO_2 < 10 ppb; and CO < 80 ppb. This air was used for continuous FTIR optical bench purging and for all experiments.

For this study, the total flow rate was set at 1 L min^{-1} unless otherwise mentioned. The flow rate was controlled by calibrated MKS mass flow controllers at 296 K and atmospheric pressure. The O_2 percentage in adsorption air compositions was adjusted between 20 and 22%. Moreover, N_2O was introduced along with NO or NO_2 for all adsorption experiments. This species was selected because it has shown no adsorption on TiO_2 into the reactor and the pipe lines up to the FTIR cell during preliminary experiments. Thus, N_2O was used as tracer to quantify NO and NO_2 adsorptions.

Table 1
FTIR detection limits of the main detected species.

Compound	Detection limit (ppbv)
NO	700
NO_2	50
N_2O	50

2.2. Adsorption/thermal regeneration reactor

Adsorption and regeneration reactor is a Pyrex glass tube characterized by 17 mm of outer diameter, 14.6 mm of inner diameter and 300 mm in length. In total length of the reactor, 120 mm in the middle was used for TiO_2 coating. For reactor coating, TiO_2 sol was prepared by stirring P25-Degussa TiO_2 particles (surface area 50 m^2/g) with Titanium tetrabutoxide solution at 353 K. The detailed description of synthesis and dip coating methods were reported by Thevenet et al. [31]. TiO_2 sol was coated on the inside wall of the Pyrex tube reactor (120 mm), first dried at 423 K for 1 h, then calcined at 723 K for 2 h in air. Glass beads were coated using the same TiO_2 sol, by stirring at 353 K for 30 min, then filtered, dried at 373 K, and calcined at 723 K for 2 h in air. Glass beads are 2 mm in diameter; they are filled in the 120 mm adsorption zone. Finally, a total amount of 75 mg TiO_2 was coated on the reactor; it was determined by weighing the reactor before and after coating. The surface area of the TiO_2 coating was determined by standard BET method with nitrogen adsorption. The determined surface area is 38 ± 3 m^2/g.

In literature, Dalton et al. [28] have reported that TiO_2 efficiently converts, under UV light, NO and NO_2 to adsorbed nitrate species. Our purpose is to investigate solely the adsorption step of NO and NO_2 on TiO_2 surface at room temperature. Therefore, in order to prevent any photocatalytically induced reaction during this study, all adsorption experiments have been performed in the absence of light by wrapping the experimental setup with aluminum foils.

2.3. Analytical device

The quantification of species at the reactor downstream was performed by FTIR spectroscopy (Thermo Scientific). A 10 m length path cell coupled with liquid nitrogen cooled MCT detector was used. FTIR spectra were collected using Result-3 software with 16 scans per spectrum and a spectral resolution of 0.5 cm^{-1}. Calibration curves and detection limits were determined from passing through the gas-cell 1 L min^{-1} of standard gases provided by Praxair. Calibration concentrations were adjusted from 10 ppbv to 200 ppmv. Similarly to background spectra, 500 scans were taken per standard spectrum. For calibration curves as well as for data processing TQ-Analyst software was used. Detection limits were evaluated as two times the Signal/Noise ratio in the regions of interest. Values of the detection limits determined for the main species identified downstream the reactor during NO_2 adsorption experiment were reported in Table 1.

Fig. 2 shows the gas phase spectra acquired during calibration using standard N_2O, NO and NO_2 cylinders balanced with N_2. As shown in Fig. 2 the framed regions were selected for quantification. For instance, N_2O has been quantified with R-branch of the band associated to the N—N stretch vibration band between 2248.4 cm^{-1} and 2223.76 cm^{-1}. For NO quantification the Q branch of R(7), R(8),

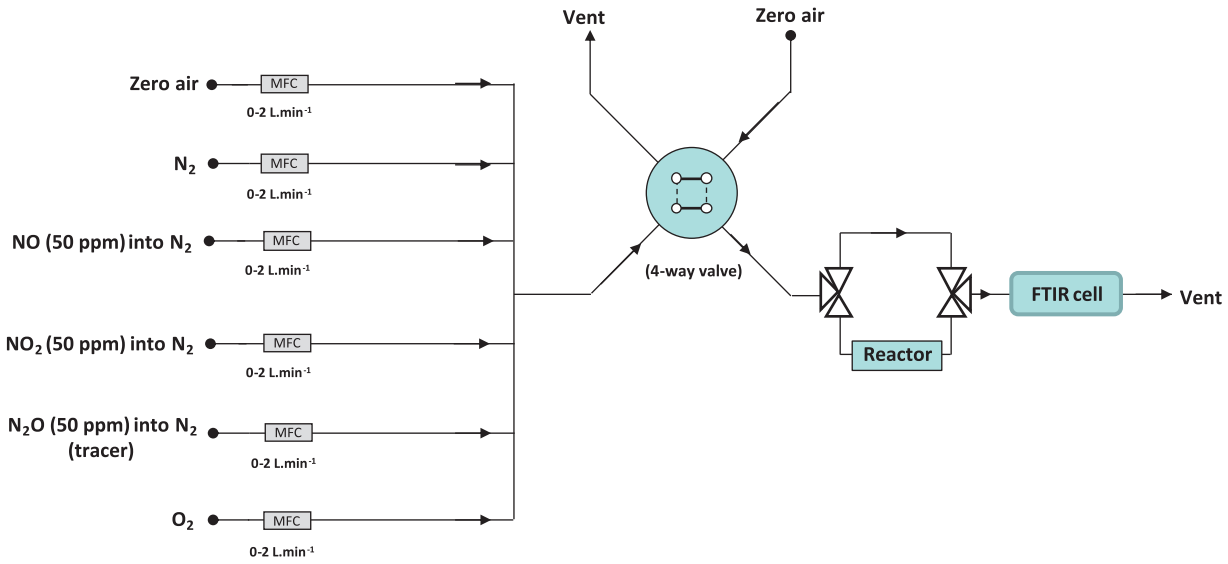

Fig. 1. General scheme of the experimental setup.

R(10) peaks respectively 1876.9–1873 cm^{-1}, 1901–1899.1 cm^{-1}, 18,586.8–1862.1 cm^{-1}, have been selected. Moreover, regions 1605.2–1604.5 cm^{-1}, 1599.8–1597 cm^{-1}, 1588.4–1584.1 cm^{-1} have been used for NO_2 quantification.

2.4. Experimental procedure

Before NO and NO_2 adsorption, the TiO_2 reactor was pre-treated under dry air at 703 K for 1 h (1 L min^{-1}) to remove the chemically adsorbed water molecules, VOCs and possible traces of adsorbed species (carbonates, nitrates, etc.). NO or NO_2 adsorption was performed at room temperature (296 K) along with tracer N_2O (3–5.5 ppm) diluted in dry air. Once NO or NO_2 breakthrough is reached, the pipe lines were flushed with pure air by by-passing the reactor. Then, the reactor was flushed under dry air in order to quantify the reversibly adsorbed fraction of NO or NO_2. Thereafter, Temperature Programmed Desorption (TPD) was performed under nitrogen, from 296 K to 703 K with a ramp of 1.1 K s^{-1}. Species in the reactor downstream were continuously monitored by FTIR spectroscopy from the beginning of NO and NO_2 adsorption to the end of thermal regeneration process.

3. Results and discussion

In order to determine the NOx adsorption mechanisms on TiO_2 at ambient conditions, NO and NO_2 adsorption have been consecutively investigated. The influence of NO_2 inlet concentration on adsorption mechanisms is discussed.

3.1. Adsorption of NO on TiO_2

NO molecule has an unpaired electron in its $2\pi^*$ anti bonding molecular orbital and can exhibit complex adsorption reactions on TiO_2 surface [32]. To investigate the NO adsorption on TiO_2 at room temperature, 10 ppm of NO were sent in the feed gas concurrently with tracer N_2O (3.5 ppm) and the resulting breakthrough curve is shown in Fig. 3.

The most striking observation from Fig. 3 is that there is no delay between NO and N_2O system mixing curves. Thus, NO shows no significant adsorption on TiO_2 at room temperature under our experimental conditions, using our analytical tools. In literature, Liu et al. [33] have discussed the possible NO adsorption mechanisms on TiO_2 anatase nanoparticle by using Density-Functional Theory (DFT). They have reported that NO can adsorbs in two modes to surface dangling Oxygen atoms: first with one bond through nitrogen, second, with two bonds through nitrogen and oxygen of NO molecule to two TiO_2 surface lattice Oxygen atoms.

In addition, they have evidenced that the second mode of adsorption is energetically favored. According to their findings NO_2, N_2O and N_2 are the expected main products by adsorbing NO on TiO_2 surface. Nevertheless, considering our detection limits, we did not monitor any evolved NO_2 and N_2O in the gas phase during NO adsorption step. This evidences that there is neither significant NO

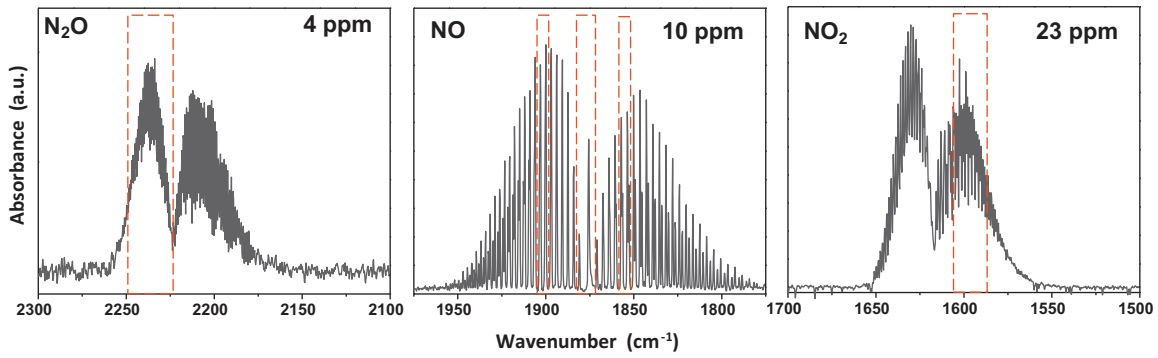

Fig. 2. FTIR gas phase spectra acquired during calibration under dry air. The framed regions were used to quantify the corresponding species.

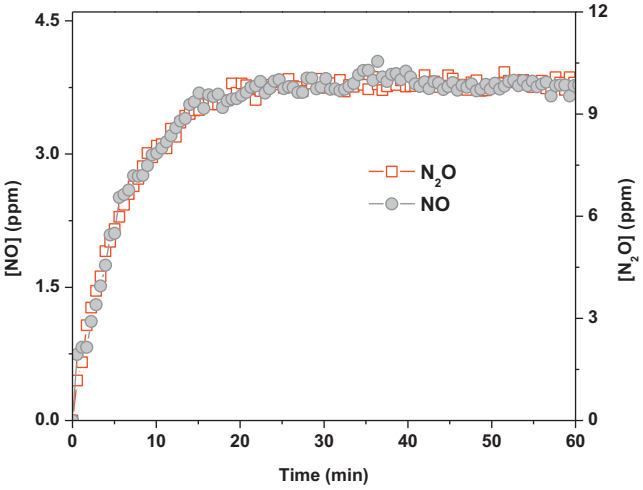

Fig. 3. Temporal profile of NO breakthrough curve on TiO_2, overlaid with N_2O tracer breakthrough curve. 10 ppm of NO and 3.5 ppm of N_2O in air were sent to reactor with a total flow rate of 1 L min^{-1}.

adsorption on TiO_2, nor NO catalytic conversion under our NO/air flowing conditions at room temperature (296 K).

After NO breakthrough, Temperature Programmed Desorption (TPD) has been performed under Nitrogen, the reactor was heated up to 703 K with the ramp of 1.1 K s^{-1}. During TPD, neither NO_2 nor NO is noticed in the reactor downstream. Similar observations are reported by Don et al. [29]. Based on our experimental results, we can draw the conclusion that NO shows no significant adsorption on TiO_2 under dry air at room temperature. As a consequence NO would not compete with other species for adsorption on TiO_2 in the case of multi pollutant gas matrixes.

3.2. NO_2 adsorption and quantification on TiO_2

To investigate the NO_2 adsorption mechanisms on TiO_2 under ambient condition, 23 ppm of NO_2 were sent in the feed gas concurrently with tracer N_2O (4.5 ppm). Prior to this experiment, the reactor was pretreated at 703 K under dry air flowing condition. The subsequent NO_2 breakthrough curve is reported in Fig. 4a. The main observations from Fig. 4a are:

(i) There is a significant delay between system mixing curve and NO_2 breakthrough curve; it evidences that NO_2 shows a quantifiable adsorption on TiO_2 under ambient condition.
(ii) NO is produced; it evidences the fact that NO_2 adsorbs on TiO_2 in a reactive way and produces NO in the gas phase.
(iii) Delayed evolution of NO leads to draw the hypothesis that the NO production probably depends on the amount of NO_2 adsorbed on TiO_2.
(iv) The tracer N_2O concentration remains constant and corresponds to input concentration, indicating that N_2O is not produced during full sequence of NO_2 adsorption. In addition, to assess this point, complementary NO_2 adsorption experiments have been performed without tracer N_2O, and evidenced that no influence of gas phase N_2O on NO_2 adsorption mechanism.

The interaction of NO_2 on TiO_2 surface has been intensively studied by authors for various experimental conditions like, (i) different NO_2 partial pressures, (ii) various temperatures ranging from 323 to 573 K [9,10,22,24,28]. Remarkably all authors have reported the production of NO in the gas phase, and formation of nitrates on TiO_2 surface.

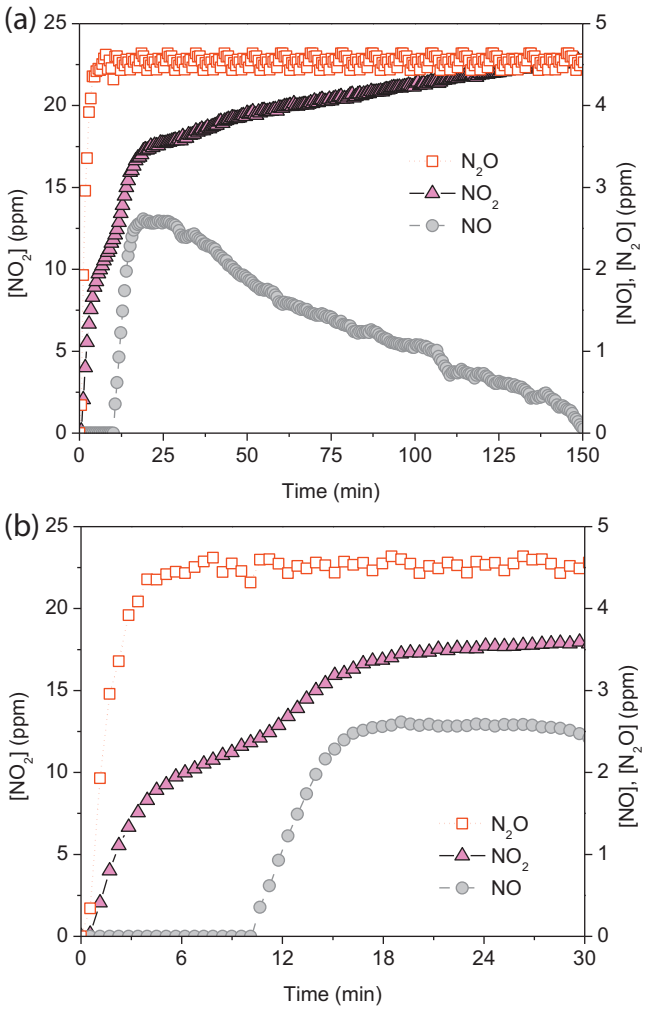

Fig. 4. Temporal profiles of NO_2 breakthrough curve on TiO_2, overlaid with N_2O tracer breakthrough curve: (a) full adsorption sequence, (b) focus on first 30 min.

As shown in Fig. 4a, NO_2 breakthrough concentration increases rapidly, followed by a slower increase with evolving NO in the gas phase. For the whole adsorption process, approximately 150 min are required to reach NO_2 steady state at the reactor downstream. The total amount of adsorbed NO_2 has been calculated by integrating the area between tracer N_2O and NO_2 breakthrough curve (Fig. 4a). Under our experimental conditions 8.3 ± 0.3 μmol/m^2 of NO_2 are adsorbed on TiO_2 after breakthrough. The uncertainty in amount of NO_2 adsorbed, and NO produced have been calculated by repeating the experiment for 4 times under the same experimental conditions. Furthermore, the monitoring of NO during NO_2 adsorption at room temperature evidences that, without any illumination of the photocatalyst, reactive adsorption occurs. The total amount of NO produced during this whole course of adsorption is quantified as 2.7 ± 0.3 μmol/m^2. Hence, the amount of NO_2 adsorbed could be more precisely denoted as NO_2 consumed in the following sections.

In order to get a better understanding on NO evolution profile, the first 30 min of NO_2 breakthrough curve is focused and presented in Fig. 4b. During the first 10 min of NO_2 adsorption, approximately 50% of feed gas NO_2 has been consumed on TiO_2. However, during this period of time NO is not noticed in the gas phase downstream the reactor. In particular, NO is produced after 10 min and reaches the maximum (2.7 ppm) within 6 min (approximately after the 16th minute of the adsorption process). Moreover, NO formation is a transient process, after 30 min, NO production drops back to zero (Fig. 4a). Therefore, the absence of NO during

first 10 min of NO_2 adsorption suggests that, NO_2 coverage on TiO_2 has to reach a threshold to initiate the NO production. As evidenced in Section 3.1, no significant amount of NO adsorbs on TiO_2 surface under our experimental conditions, thus, it can be assumed that all NO produced during adsorption has been monitored in the gas phase. The total amount of NO produced represents 33% of total consumed NO_2 along the complete adsorption sequence. Therefore, the ratio between $NO_{2(consumed)}$ and $NO_{(produced)}$ is 3:1. Similar findings were reported by Despres et al. [34] and Haubrich et al. [24]. Despres et al. [34] have investigated the NO_2 storage capacity on TiO_2 at 473 K, for 500 ppm of NO_2 inlet concentration, and reported a slightly lower NO_2 storage capacity of 2.2 μmol/m^2 on TiO_2. This lower adsorption phenomenon can be attributed to the adsorption performed at higher temperature, nevertheless, the authors also reported the ratio of 3:1 between $NO_{2(consumed)}$ and $NO_{(produced)}$ which is in good agreement with our findings.

Haubrich et al. [24] and Rodriguez et al. [25] have investigated NO_2 adsorption steps on TiO_2 (110) under Ultra High Vacuum (UHV) conditions, by using photoemission and XANES experiments as well as theoretical density functional (DFT) calculations. They have reported that NO_2 adsorbs on TiO_2, and produce one NO in the gas phase through disproportionation reaction between two adsorbed NO_2 molecules by leaving one NO_3 on TiO_2 surface. Furthermore, Rodriguez et al. [25] reported the fact that the adsorbed NO_3 is formed by disproportionation reaction and not by direct reactive adsorption of NO_2 on O-vacancy sites on TiO_2 surface, and the remaining adsorbed NO_3 is electro neutral in nature. Besides, they also reported the migration of O vacancies from subsurface to the surface during NO_2 adsorption. In addition, authors suggested the same mechanism for other metal oxides like CeO_2, CuO, ZnO, Cr_2O_3 and Fe_2O_3. In brief, a NO_2 adsorption mechanism on TiO_2 surface at room temperature is generally reported as follows, without any precise species quantification support:

$$NO_2(g) \rightleftharpoons NO_2(ads) \quad (1)$$

$$2NO_2(ads) \rightleftharpoons NO_3(ads) + NO(g) \quad (2)$$

Considering Eq. (2), the expected ratio between $NO_{2(consumed)}$ and $NO_{(produced)}$ is 2:1, which is clearly not in accordance with our experimental quantitative measurements (3:1) and other authors [34]. Therefore, the general mechanism suggested by Rodriguez et al. [25] for NO_2 adsorption on TiO_2 at room temperature should be reconsidered.

On the other hand Apostolescu et al. [35] have investigated the NO_2 adsorption mechanisms on Al_2O_3 at 323 K using Diffuse Reflectance Infrared Fourier Transformation spectroscopy (DRIFTS). On Al_2O_3 surface, NO_2 adsorbs in a reactive way and produces NO_3 in adsorbed phase and NO in the gas phase. In particular, they have reported the ratio of about 3:2:1 between $NO_{2(consumed)}$, $NO_{2(desorbed)}$ by TPD performed after NO_2 adsorption and $NO_{(produced)}$ in the gas phase during NO_2 adsorption, respectively. Furthermore, the authors have confirmed the fact that, the NO formation proceeds through three successive reactions as follows:

(i) Two adsorbed NO_2 undergo a disproportionation reaction and produce NO_3^- and NO^+ on Al_2O_3 surface,
(ii) NO^+ is highly reactive; hence it reacts with Al_2O_3 lattice O^{2-} and produce NO_2^-, and
(iii) NO_2^- further reacts with another adsorbed NO_2 and produces adsorbed NO_3^- and gas phase NO.

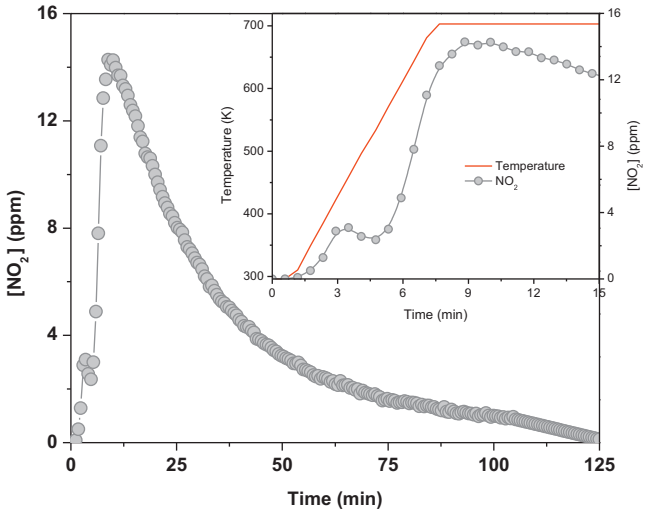

Fig. 5. Temporal profile of NO_2 desorbed during temperature programmed desorption (TPD) of NO_2 (23 ppm) saturated TiO_2 surface. Thermal treatment was performed under Nitrogen (1 L min^{-1}) with a temperature ramp of 1.1 K s^{-1}. Temperature ramp is displayed in the insert which is a focus on the first 15 min of TPD.

Therefore, we propose a similar mechanism for NO_2 adsorption on TiO_2 at room temperature and under dry air flowing condition as follows:

$$2NO_2(ads) \rightleftharpoons NO_2^- + NO^+(ads) \quad (3)$$

$$NO + O^{2-}(TiO_{2Surfacelatice}) \rightleftharpoons NO_2^-(ads) \quad (4)$$

$$NO_2^-(ads) + NO_2(ads) \rightleftharpoons NO_3^-(ads) + NO(g) \quad (5)$$

According to this mechanism, the global Equation of NO_2 adsorption can be written by summing up Eqs. (3)–(5) as denoted in Eq. (6):

$$3NO_2(ads) \rightleftharpoons 2NO_3^-(ads) + NO(g) \quad (6)$$

As reported in Eq. (6), three NO_2 molecules have been involved in two consecutive disproportionation reactions to produce one NO in the gas phase. Thus, the theoretical ratio is 3:1 between $NO_{2(consumed)}$ and $NO_{(produced)}$, which is in agreement with our quantitative measurements performed downstream the adsorption reactor. Moreover, as shown in Eq. (6), two NO_3^- species have been stored on TiO_2 to produced one NO in the gas phase. Therefore, this proposed mechanism could be quantitatively assessed by determining the total amount of NO_3^- stored on TiO_2 surface. Hence, the NO_2 saturated TiO_2 has been subjected to Temperature Programmed Desorption (TPD); results are discussed in the following section.

3.3. Temperature programmed desorption of NO_2 saturated TiO_2 surface

To assess the proposed NO_2 adsorption mechanisms on TiO_2 at room temperature (Eqs. (3)–(6)), TPD have been performed on NO_2 saturated TiO_2 under N_2 flow. Prior to TPD, the reactor was thoroughly flushed under N_2 at 296 K. It was found that neither NO and nor NO_2 have been detected in the reactor downstream, indicating that all consumed NO_2 has been strongly adsorbed on TiO_2 at room temperature. During TPD, the total N_2 flow has been kept constant at 1 L min^{-1}. The NO_2 saturated TiO_2 reactor was heated up to 703 K, with a heating rate of 1.1 K s^{-1}. The obtained temporal profile of monitored species is reported in Fig. 5. The most important observation is that only NO_2 has been monitored during the

course of thermal desorption. In addition, TPD has been performed until NO_2 concentration reaches zero in the reactor downstream, making possible the complete quantification of NO_2 desorbed.

As shown in Fig. 5, NO_2 desorbs in two distinct peaks (inserted figure with temperature profile). First, very narrow peaks centered approximately at 3 min, and second a broad peak at 9 min. These two peaks have been quantified separately and discussed. The first peak at 3 min can be attributed to desorption of weakly adsorbed NO_2^-, or NO_3^- from TiO_2 surface; the corresponding desorption temperature is low: 450 K. The broad peak, at 9 min, corresponds to the strongly adsorbed species, desorbing at higher temperature, more than 580 K. Haubrich et al. [24] have evidenced the decomposition of NO_3^- over 520 K by in situ FTIR spectroscopy. Furthermore, according to our proposed mechanisms, the strongly adsorbed NO_3^- species are produced by consuming the surface lattice O^{2-} (Eqs. (4) and (5)). Therefore, during thermal treatment it is likely to produce NO_2 by leaving O^- to TiO_2 surface lattice. By considering our proposed mechanisms, the broad second peak can be attributed to the decomposition of chemisorbed NO_3^- into NO_2 in the gas phase as mentioned in Eq. (7).

$$NO_3^-(ads) \xrightarrow{\Delta} O(ads) + NO_2(g) \quad (7)$$

Approximately 0.2 ± 0.1 μmol/m^2 of NO_2 have been quantified by integrating the first small peak desorbed at 450 K. In addition, 5.4 ± 0.1 μmol/m^2 of NO_2 have been quantified from the second peak integration. Therefore, approximately 5.6 ± 0.1 μmol/m^2 of NO_2 have been removed from TiO_2 surface along the TPD, corresponding to 67% of total consumed NO_2. Thus, for 23 ppm of inlet concentration, the ratio between consumed NO_2 and thermally desorbed NO_2 can be written as 3:2 (Fig. 5). Furthermore, assuming the distinction between both peaks, the TPD profile shows that, 97% of thermally desorbed species are represented by the second peak. This shows that 97% of consumed NO_2 have been stored as strongly adsorbed NO_3^- on TiO_2 surface. As a conclusion, from a qualitative and a quantitative point of view, NO_2 reactive adsorption on TiO_2 surface could be described by Eqs. (3)–(5).

However, a special attention has been paid to understand the influence of NO_2 adsorption time (i.e.) NO_2 coverage on adsorption mechanism, series of experiments have been performed for various NO_2 adsorption time, and corresponding TPD profiles are discussed in the following section.

3.3.1. *Investigation of NO_2 adsorption time on mechanism advancement*

According to our proposed mechanism, two adsorbed NO_3^- species have been produced in Eqs. (3) and (5). Thus, only one NO_2 desorption peaks is expected during TPD under N_2. Nevertheless, as we evidenced in Section 3.3, NO_2 has been desorbed in two distinct peaks centered at 450 K and above 580 K, indicating that two different NO_3^- species were adsorbed on TiO_2 surface at room temperature. Furthermore, approximately 97% of total consumed NO_2 has been desorbed in a broad second peak certainly at higher temperature (above 580 K). Therefore it can be suggested that, the NO_2 adsorption time would significantly modify the nature of adsorbed species, especially the amount of NO_3^- produced and adsorbed in Eq. (3). To assess this hypothesis, series of NO_2 adsorption experiments have been performed for two different adsorption time, typically (i) adsorption for 10 min, (ii) adsorption up to breakthrough, with 23 ppm of NO_2 inlet concentration.

Firstly, considering Eqs. (3) and (4), and NO formation time (Fig. 4b), NO_2 adsorption has been performed for only 10 min in order to prevent NO formation. As expected, during the 10 min of NO_2 adsorption, except NO_2, no other species have been monitored

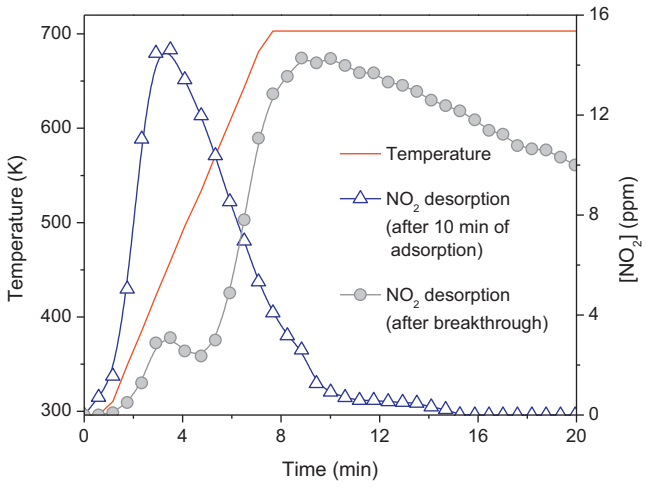

Fig. 6. Influence of NO_2 adsorption duration (150 min breakthrough, or 10 min adsorption) on the temporal profile of NO_2 desorbed during temperature programmed desorption (TPD). Thermal treatment was performed under Nitrogen (1 L.min^{-1}), with a temperature ramp of 1.1 K s^{-1}.

in the reactor downstream. This evidences that, NO_2 adsorption for 10 min does not initiate the disproportionation reaction leading to NO production in the gas phase as proposed in Eq. (5).

Secondly, after 10 min adsorption, the reactor has been thoroughly flushed at ambient temperature under N_2. It was noticed that no significant amount of NO_2 desorbed. Thus, even for partial surface coverage ($\theta < 0.2$), NO_2 is irreversibly adsorbed on TiO_2 at room temperature.

Thirdly, thermal desorption has been performed under N_2. The corresponding NO_2 thermal desorption temporal profile is compared in Fig. 6 with the profile obtained as NO_2 breakthrough is achieved. The desorption temperature profile is also depicted in Fig. 6. As reported in Fig. 6, adsorption being performed for only 10 min, NO_2 is thermally desorbed in a single peak centered at 450 K, which corresponds to the first NO_2 desorption peak observed as NO_2 was adsorbed until breakthrough. It evidences that the adsorbed species produced by Eqs. (3) and (4) remain weakly bonded to the surface. The involvement of Equation (5) in the mechanism is clearly controlled by TiO_2 surface coverage. Eq. (5) leads to the formation of NO in the gas phase, and also corresponds to the conversion of weakly bonded surface species produced by Eqs. (3) and (4) into strongly bonded NO_3^- species. This evidences that the NO_2 adsorption time (surface coverage) controls the adsorption mechanisms and simultaneously modifies the nature of adsorbed species.

In order to investigate further the proposed mechanism, the sensitivity of NO_2 consumed, NO formation and NO_2 desorption (TPD) to NO_2 inlet concentration has been evaluated. Results are reported in the following section.

4. Influence of NO_2 inlet concentrations

To investigate the influence of NO_2 inlet concentrations on adsorption mechanism, NO_2 adsorption has been studied at room temperature by varying the inlet concentration of NO_2 from 11 to 52 ppm. The various NO_2 inlet concentrations have been prepared by adjusting the NO_2 flow rate with pure Oxygen, Nitrogen and Zero air. The adsorption was performed during 150 min for all studied adsorption sequences. Temporal profiles of the species monitored in the reactor downstream during adsorption are reported in Fig. 7a and b.

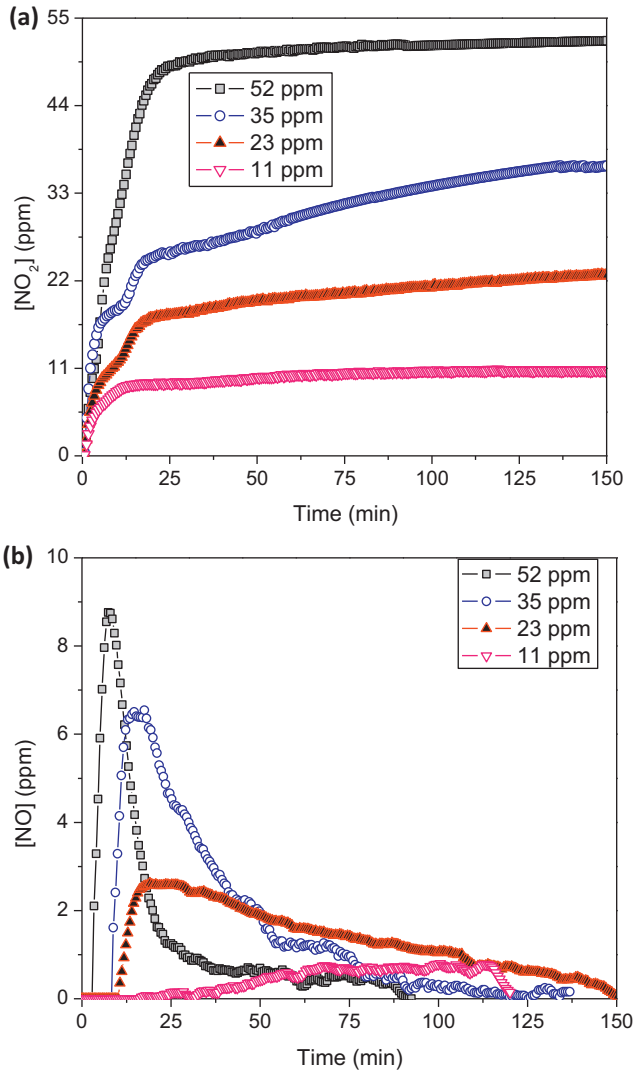

Fig. 7. Temporal evolutions of a) NO_2, and b) NO concentrations at the reactor downstream during NO_2 adsorption for NO_2 inlet concentrations ranging from 11 to 52 ppm.

4.1. Quantification of NO_2 consumption and NO production for various NO_2 inlet concentrations

Fig. 7a shows the NO_2 breakthrough curves as a function of adsorption time for various NO_2 inlet concentrations; Fig. 7b displays the corresponding NO profiles. Roughly, irrespectively of NO_2 inlet concentrations, NO_2 adsorbs on TiO_2 in a reactive way since NO is measured downstream the reactor. However, temporal profiles appear to be highly sensitive to NO_2 inlet concentrations.

First, a special attention should be paid to NO formation profiles in order to get better understanding of the influence of NO_2 inlet concentrations on adsorption mechanisms. As shown in Fig. 7b, the maximum of NO formation decreases from 9 to 0.8 ppm with decreasing the NO_2 inlet concentrations from 52 to 11 ppm. Moreover, NO initial formation time also varies with NO_2 inlet concentration. In Section 3.2, the hypothesis of a threshold limit of adsorbed species to initiate NO formation was proposed. Hence, to asses this hypothesis the amount of NO_2 consumed for corresponding time to detect NO using FT-IR spectroscopy has been calculated and reported in Table 2.

Table 2 shows the influence of NO_2 inlet concentrations on NO initial formation time, and the corresponding amount of consumed NO_2. NO initial formation time increases from 4 to 65 min, by decreasing the NO_2 inlet concentrations from 52 to 11 ppm. However, for all employed NO_2 inlet concentrations, 3 ± 0.2 μmol/m^2 of NO_2 are consumed on TiO_2 as NO production starts. This result confirms that the amount of 3 ± 0.2 μmol/m^2 of adsorbed NO_2 can be considered as a threshold limit to initiate Eq. (5) on TiO_2 surface. This result is in good accordance with the mechanism proposed in Section 3.2. Reaction steps depicted by Eqs. (3) and (4) do not depend on NO_2 inlet concentrations. NO formation is initiated provided that a surface coverage by adsorbed species produced from Eqs. (3) and (4) is reached. It suggests that NO_2 inlet concentration only affects the kinetic of the reactive adsorption, and in particularly the surface coverage kinetic, not the mechanism itself.

Table 2
Influence of NO_2 inlet concentrations on NO initial formation time and corresponding amount of NO_2 consumed.

NO_2 inlet concentration (ppm)	Initial NO formation time (min)	Amount of NO_2 consumed (μmol/m^2) as NO formation starts
52	4	3.0
35	10	3.0
23	13	2.8
11	65	2.8

Table 3 summarizes the influence of NO_2 inlet concentrations on the total amount of NO_2 consumed, total amount of NO produced during the adsorption sequences, and the ratio between $NO_{2(consumed)}$ and $NO_{(produced)}$. The total amount of consumed NO_2 and produced NO has been calculated using the methods described in Section 3.2. Both data series follow the same trend and the ratio between NO_2 consumed and NO produced are around 3:1 for all employed NO_2 inlet concentrations expect 11 ppm. For 11 ppm inlet concentration the ratio is 3.5:1. This 16% deviation can be attributed to the more NO_2^- and/or NO_3^- storage as depicted in Eqs. (3) and (4) rather than strongly adsorbed NO_3^- formation by disproportionation reaction as mentioned in Eq. (5). This hypothesis is be assessed by thermal desorption experiment in the following Section 4.2. However, the ratio of 3:1 between $NO_{2(consumed)}$ and $NO_{(produced)}$ for inlet concentrations ranging from 23 to 52 ppm evidences that the proposed mechanism is still valid.

Moreover, maximum values are obtained with 35 ppm NO_2 inlet concentration for both NO_2 consumed and NO produced. On the one hand, from 11 to 35 ppm, the linear increase in NO_2 consumption on TiO_2 surface can be explained by a classical behavior corresponding to Langmuir isotherm. On the second hand, the consumed NO_2 decreases, when NO_2 gas phase concentration is raised over 35 ppm. At this stage it is difficult to interpret the decrease in NO_2 consumption without TiO_2 surface analysis. However, from the proposed mechanism, one possibility could be the TiO_2 surface poisoning by NO_3^-species produced by Eq. (3). In particular, this adsorbed NO_3^- species probably hinders the availability of NO_2 adsorption sites; consequently the total amount of NO_2 consumed is decreased. This hypothesis could be confirmed by surface characterization using Transmission FTIR. Thus, the diffusion of NO_3^- is required to make possible the further adsorption of NO_2. As discussed earlier, the increase of NO_2 inlet concentration tends to promote the reactive adsorption kinetic. Then, over 35 ppm of NO_2 in the gas phase, NO_3^- diffusion toward secondary adsorption sites probably becomes a limiting step regarding NO_2 adsorption. As a consequence, NO_2 consumed is diminished as well as NO produced. Once again, the proposed mechanism is still valid, this hypothesis on self poisoning would only affect the kinetics of Equation (3) and (4).

Table 3
Amounts of NO_2 consumed and NO produced per sorbent surface unit for various NO_2 inlet concentrations. All experiments were performed at 296 K, under dry air.

NO_2 inlet concentration (ppm)	NO_2 adsorption till breakthrough		$NO_{2(consumed)}/NO_{(produced)}$
	Total NO_2 consumed (μmol/m^2)	Total NO produced (μmol/m^2)	
52	8.3	2.8	3.0
35	12	3.9	3.0
23	8.2	2.7	3.0
11	2.2	0.6	3.5

4.2. Thermal regeneration of NO_2 saturated TiO_2 surface

The amount of species stored on TiO_2 surface as a function of NO_2 inlet concentration has been characterized by TPD under N_2 flow. NO_2 is the only species monitored at the reactor outlet during TPD. Similarly to Fig. 5, and irrespectively of NO_2 inlet concentration, two NO_2 peaks are evidenced during TPD. Fig. 8 shows the amount of NO_2 desorbed in different peaks for various NO_2 inlet concentrations. As seen from Fig. 8, the amount of NO_2 desorbed by the first peaks decreases with increasing the NO_2 inlet concentrations; on the contrary the amount of NO_2 desorbed by 2nd peak increases with increasing the NO_2 inlet concentrations. Considering the temperature of the peak maximum (450 K), the first peak corresponds to weakly adsorbed NO_2^- and/or NO_3^- as discussed in Section 3.3.1, whereas, the second peak (above 580 K) corresponds to desorption of thermally decomposed NO_3^- species to NO_2. In particular, the amount of NO_2 desorbed in the second peak remains the major species especially over 23 ppm inlet concentration where the contribution of weakly adsorbed NO_2^- and/or NO_3^- remains lower than 3% of the total desorbed NO_2. Nevertheless, the contribution of weakly adsorbed NO_2^- and/or NO_3^- tends to increase significantly as NO_2 gas phase concentration is decreased. For 11 ppm NO_2 inlet concentration, the amount of NO_2 desorbed by first peak (at 450 K) contributes to 45% of total consumed NO_2. It clearly evidences that, for 11 ppm NO_2 inlet concentration, around 45% of adsorbed NO_2 has been stored as weakly adsorbed NO_2^- and/or NO_3^- as depicted in Eqs. (3) and (4). This is in accordance with the hypothesis proposed in Section 4.1 for the higher ratio of 3.5:1 between $NO_{2(consumed)}$ and $NO_{(produced)}$ for 11 ppm. In conclusion, the proposed mechanism is sensitive to the NO_2 gas phase concentrations. In particular, Eqs. (3) and (4) are not mainly influenced by NO_2 gas phase concentration, whereas the disproportionation reaction (i.e.) Eq. (5) is modified by the NO_2 gas phase concentration.

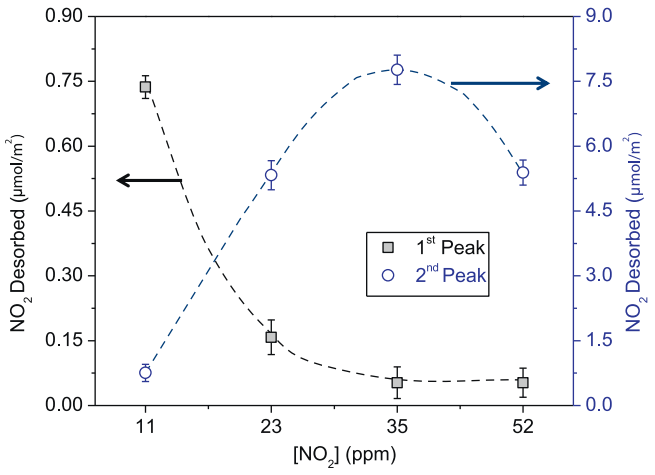

Fig. 8. Evolution of NO_2 amounts desorbed per sorbent surface unit as a function of NO_2 inlet concentrations. The two desorption peaks have been integrated and their evolutions are displayed separately. Thermal treatment was performed under Nitrogen (1 L min^{-1}), with temperature ramp of 1.1 K s^{-1}.

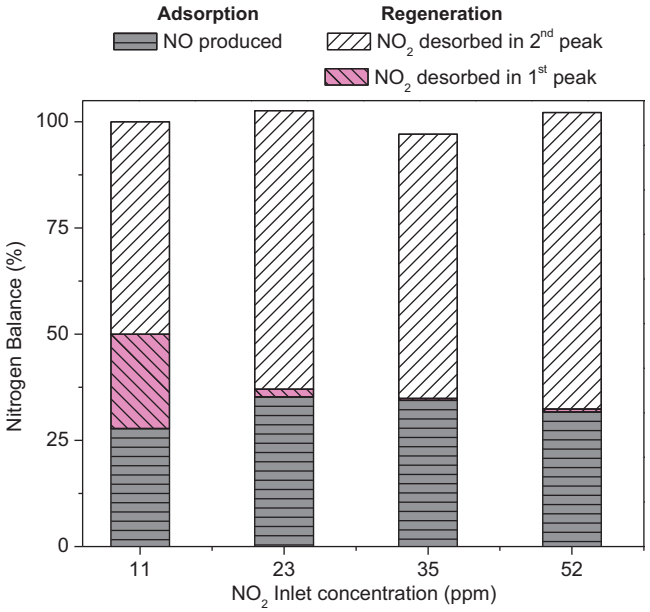

Fig. 9. Total nitrogen balance obtained by adsorption and TPD process for various NO_2 inlet concentrations.

The relative contribution of adsorption modes could be investigated further using lower concentrations of NO_2 and transmission FTIR spectroscopy. The temporal profile of total desorbed NO_2 is coherent with the one of consumed NO_2. Based on this value, Nitrogen balances can be evaluated.

The total nitrogen balance has been calculated for each NO_2 inlet concentration by considering the amount of NO_2 consumed during the adsorption step as reference. Then, the relative contributions of (i) NO produced during adsorption, (ii) weakly adsorbed NO_2^- and/or NO_3^- desorbed as NO_2 by TPD in the first peak and (iii) NO_3^- desorbed by TPD as NO_2 in the second peak have been determined. Calculated values are reported in Fig. 9 for each NO_2 inlet concentration. As shown in Fig. 9, for all employed inlet concentrations, the nitrogen balance obtained by whole adsorption/desorption process remains approximately 100 ± 3%. This confirms that all the Nitrogen based species involved in the mechanism have been monitored and quantified.

5. Conclusions

In this paper, the adsorption of NO and NO_2 on TiO_2 at room temperature has been investigated. TiO_2 can be considered as a relevant material for adsorption and plasma catalytic oxidation of VOCs, owing to oxidative surface properties even during the adsorption step. It was evidenced that, NO would not compete with other VOCs for adsorption on TiO_2 at room temperature, since NO has shown no significant adsorption on TiO_2 at room temperature and under our experimental conditions. On the other hand, NO_2 may significantly influence the VOC adsorption and mineralization on TiO_2 surface. We have evidenced that, as soon as a threshold

surface coverage is reached, at room temperature, NO_2 adsorbs in a reactive way on TiO_2 by evolving NO in the gas phase. A new NO_2 adsorption mechanism on TiO_2 at room temperature has been proposed and evidenced by quantitative measurements performed downstream the reactor. Furthermore, the proposed mechanism has been tested and validated for various NO_2 inlet concentrations. The main conclusions from NO_2 adsorption mechanism on TiO_2 at room temperature are:

(1) Three adsorbed NO_2 molecules on TiO_2 produce two NO_3^- on TiO_2 surface and evolve one NO in the gas phase.
(2) The ratio between consumed NO_2, desorbed NO_2 by TPD after adsorption and produced NO during NO_2 adsorption can be written as 3:2:1 on the investigated NO_2 inlet concentration range.
(3) NO_2 adsorption time, i.e. TiO_2 surface coverage, significantly modifies the nature of adsorbed species at room temperature.
(4) NO formation time is mainly controlled by NO_2^- and NO_3^- surface coverage rather than NO_2 inlet concentration. A surface coverage threshold has been evidenced for NO formation.
(5) At room temperature, for higher NO_2 gas phase concentration, typically above 35 ppm, the total amount of consumed NO_2 is decreased, owing to self poisoning by adsorbed NO_3^- species.

Acknowledgements

The authors greatly acknowledge the French National Research Agency (ANR) for its financial support. Experiments have been performed in the framework of the ANR Blanc-RAMPE project. The authors would like to express special thanks to Prof. Daniel BIANCHI and Dr. Olivier GUAITELLA for their comments, discussions and supports.

References

[1] B.F. Yu, Z.B. Hu, M. Liu, H.L. Yang, Q.X. Kong, Y.H. Liu, International Journal of Refrigeration 32 (2009) 3–20.
[2] K. Skalska, J.S. Miller, S. Ledakowicz, Science of the Total Environment 408 (2010) 3976–3989.
[3] A. Maudhuit, C. Raillard, V. Héquet, L. Coq, J. Sablayrolles, L. Molins, Chemical Engineering Journal 170 (2011) 464–470.
[4] F. Thevenet, O. Guaitella, E. Puzenat, J.M. Herrmann, A. Rousseau, C. Guillard, Catalysis Today 122 (2007) 186–194.
[5] C.H. Tsai, H.H. Yang, C.J.G. Jou, H.M. Lee, Journal of Hazardous Materials 143 (2007) 409–414.
[6] L. Sivachandiran, F. Thevenet, P. Gravejat, A. Rousseau, Chemical Engineering Journal 214 (2013) 17–26.
[7] H.H. Kim, S.M. Oh, A. Ogata, S. Futamura, Applied Catalysis B: Environmental 56 (2005) 213–220.
[8] R.M. Alberici, M.C. Canela, M.N. Eberlin, W.F. Jardim, Applied Catalysis B: Environmental 793 (2000) 1–9.
[9] T.H. Lim, S.M. Jeong, S.D. Kim, J. Gyenis, Journal of Photochemistry and Photobiology A 134 (2000) 209–217.
[10] H. Wang, Z. Wu, W. Zhao, B. Guan, Chemosphere 66 (2007) 185–190.
[11] O. Debono, F. Thevenet, P. Gravejat, V. Hequet, C. Raillard, L. Lecoq, N. Locoge, Applied Catalysis B: Environmental 106 (2011) 600–608.
[12] H. Park, W. Choi, Journal of Physical Chemistry B 108 (2004) 4086–4093.
[13] S. Bahri, C.M. Jonsson, C.L. Jonsson, D. Azzolini, D.A. Sverjensky, R.M. Hazen, Environmental Science & Technology 45 (2011) 3959–3966.
[14] F. Thevenet, J. Couble, M. Brandhorst, J.L. Dubois, E. Puzenat, C. Guillard, D. Bianchi, Plasma Chemistry and Plasma Processing 30 (2010) 489–502.
[15] R. Alvarez, M. Weilenmann, J.Y. Favez, Atmospheric Environment 42 (2008) 4699–4707.
[16] J.V. Durme, J. Dewulf, W. Sysmans, C. Leys, H.V. Langenhove, Applied Catalysis B: Environmental 74 (2007) 161–169.
[17] X. Fan, T.L. Zhu, M.Y. Wang, X.M. Li, Chemosphere 75 (2009) 1301–1306.
[18] H.H. Kim, Plasma Process and Polymers 1 (2004) 91–110.
[19] C.J. Weschler, A.T. Hodgson, J.D. Wooley, Environmental Science & Technology 28 (1994) 2120.
[20] A. Chaloulakou, I. Mavroidis, I. Gavriil, Atmospheric Environment 42 (2008) 454–465.
[21] S. Matsuda, H. Hatano, A. Tsutsumi, Chemical Engineering Journal 82 (2001) 183–188.
[22] F.L. Toma, G. Bertrand, D. Klein, C. Coddet, Environmental Chemistry Letters 2 (2004) 117–121.
[23] C. Morterra, G. Ghiotti, E. Garrone, E. Fisicaro, Journal of the Chemical Society, Faraday Transactions 1 (76) (1980) 2102.
[24] J. Haubrich, R.G. Quiller, L. Benz, Z. Liu, C.M. Friend, Langmuir 26 (2010) 2445–2451.
[25] J.A. Rodriguez, T. Jirsak, G. Liu, J. Hrbek, J. Dvorak, A. Maiti, Journal of the American Chemical Society 123 (2001) 9597–9605.
[26] J. Abad, O. Bohme, E. Roman, Langmuir 23 (2007) 7583–7586.
[27] A. Folli, S.B. Campbell, J.A. Anderson, D.E. Macphee, Journal of Photochemistry and Photobiology A 220 (2011) 85–93.
[28] J.S. Dalton, P.A. Janes, N.G. Jones, J.A. Nicholson, K.R. Hallam, G.C. Allen, Environmental Pollution 120 (2002) 415–422.
[29] D.C. Sorescu, C.N. Rusu, J.T. Yates, Journal of Physical Chemistry B 104 (2000) 4408–4417.
[30] W.S. Epling, A. Yezerets, N.W. Currier, Applied Catalysis B: Environmental 74 (2007) 117–129.
[31] F. Thevenet, O. Guaitella, J.M. Herrmann, A. Rousseau, C. Guillard, Applied Catalysis B: Environmental 61 (2005) 58–68.
[32] J.A. Rodriguez, T. Jirsak, J.Y. Kim, J.Z. Larese, A. Maiti, Chemical Physics Letters 330 (2000) 475.
[33] J. Liu, Q. Liu, Applied Surface Science 258 (2012) 8312–8318.
[34] J. Despres, M. Koebel, O. Kröcher, M. Elsener, A. Wokaun, Applied Catalysis B: Environmental 43 (2003) 389–395.
[35] N. Apostolescu, T. Schröder, S. Kureti, Applied Catalysis B: Environmental 51 (2004) 43–50.